

## A HIGH-RESOLUTION NEUTRAL-HYDROGEN STUDY OF THE GALAXY M81

S. T. GOTTESMAN

Department of Physics and Astronomy, University of Florida, Gainesville

AND

L. WELIACHEW

Owens Valley Radio Observatory, California Institute of Technology; and  
 Département de Radioastronomie, Observatoire de Meudon, France

Received 1974 April 23; revised 1974 July 23

### ABSTRACT

A 2' synthesis of M81 (NGC 3031) has been made in the 21-cm neutral-hydrogen emission line. In addition to the interferometric data, a single-dish measurement provided information about the large-scale structure. One-third of the H I observed appears to be divorced from the main body of the galaxy and shows large non-circular motions. The satellite system DDO 66/Ho IX has been observed with an indicative total mass of  $5 \times 10^9 M_{\odot}$  of which 10-20 percent is H I, assuming a distance of 3.25 Mpc to M81. The neutral-hydrogen content of this dwarf irregular galaxy is very high for its luminosity when compared with normal galaxies. The diffuse ring located north of M81 and first noted by Arp has  $\sim 1.2 \times 10^9 M_{\odot}$  of H I associated with it. The line-of-sight velocities in this feature are totally inconsistent with rotation in the main plane of M81.

A rotation curve was established for M81, and within 20 kpc of the center a mass of  $1.1 \times 10^{11} M_{\odot}$  is found. The neutral-hydrogen mass in M81 is  $4.9 \times 10^9 M_{\odot}$ . The disk of M81 shows strong noncircular motion in the vicinity of DDO 66/Ho IX. The spiral arms of the galaxy are resolved with a width of  $\sim 2$  kpc at a radial distance of 7-10 kpc from the center. In the same region the intrinsic contrast of the gas density of the arms is 3:1-5:1. Employing our new results, a density-wave model is discussed which appears to be in better agreement with the structure of the galaxy than the model using older optical data proposed by Shu *et al.* The kinematics of M81, as derived from our study, do not show the systematic pattern of noncircular velocities expected from the density-wave theory. However, the magnitude of these noncircular terms expected from our density-wave model are too small to be detected where the H I arms are well resolved.

*Subject headings:* galaxies, individual — galaxies, motions in — 21-cm radiation

### I. INTRODUCTION

High-resolution studies of the dynamics and distribution of neutral hydrogen in galaxies are important, for information is provided about a wide range of galactic properties. In this paper we report on a study of the galaxy M81 (NGC 3031), which is a large Sb system that is relatively near (Tammann and Sandage 1968 derive a distance of 3.25 Mpc to the M81 group) and inclined by  $58^{\circ}$  to the sky plane. Thus, the study of the spiral structure of this galaxy is facilitated at modest resolutions.

The galaxy is also very close to M82, and Arp (1965) has postulated an electromagnetic interrelationship between the two systems. Furthermore, M81, M82 and NGC 3077 form a triple system enveloped in a tenuous H I halo (Roberts 1972). Thus, a neutral hydrogen study of any of these galaxies may yield information about the structure and kinematics of this intergalactic medium and of any galactic interactions.

### II. OBSERVATIONS AND REDUCTION METHODS

Observations of the galaxy M81 have been made using the two-element interferometer of the Owens Valley Radio Observatory. We have synthesized a resolution of 2' which is equivalent to 1.9 kpc at a distance of 3.25 Mpc. The general properties of this

interferometer have been described in detail by Rogstad and Shostak (1971). We have previously described our procedures with respect to concomitant observations of M51 (Weliachew and Gottesman 1973). We will, therefore, only note here the important instrumental parameters. The incremental telescope spacing was 100 feet ( $144 \lambda$ ), and as this was also the closest spacing employed, structure within any channel  $\sim 11'$  in size will be 50 percent resolved. The largest spacing at which observations were made was 800 feet ( $1152 \lambda$ ) providing a synthesized, almost circular, beam of 2' half-power width. The first strong grating response synthesized was  $\sim 25.5'$  from the beam center. The total observing time on the galaxy was 76 hours.

Information about the H I profile was provided by a filter-bank system of 23 contiguous, 100-kHz ( $21.1 \text{ km s}^{-1}$ ) channels. A broad-band 6.05-MHz filter provided nominal continuum data that was simultaneously recorded. The rms noise fluctuations in each 100-kHz bandwidth after 15 minutes of integration was 0.1-0.15 f.u.<sup>1</sup> The local oscillator was maintained at a fixed Doppler velocity<sup>2</sup> of  $-36 \text{ km s}^{-1}$ .

The data are initially presented in the form of single-channel velocity maps of the Doppler-shifted H I in

<sup>1</sup> 1 flux unit equals  $10^{-26} \text{ W m}^{-2} \text{ Hz}^{-1}$ .

<sup>2</sup> All velocities quoted in this paper are with respect to the Sun.

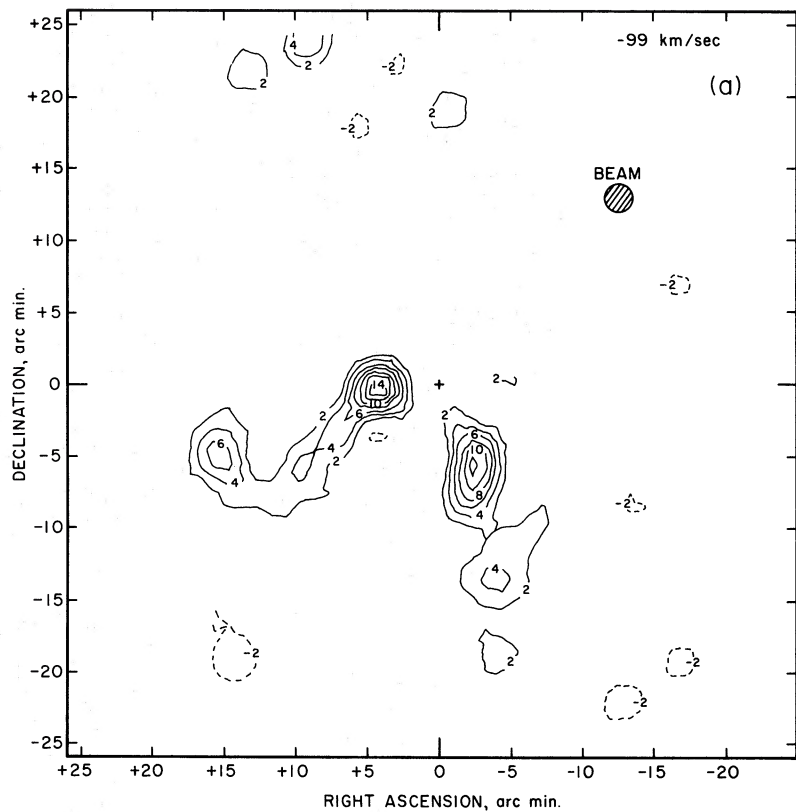


FIG. 1a

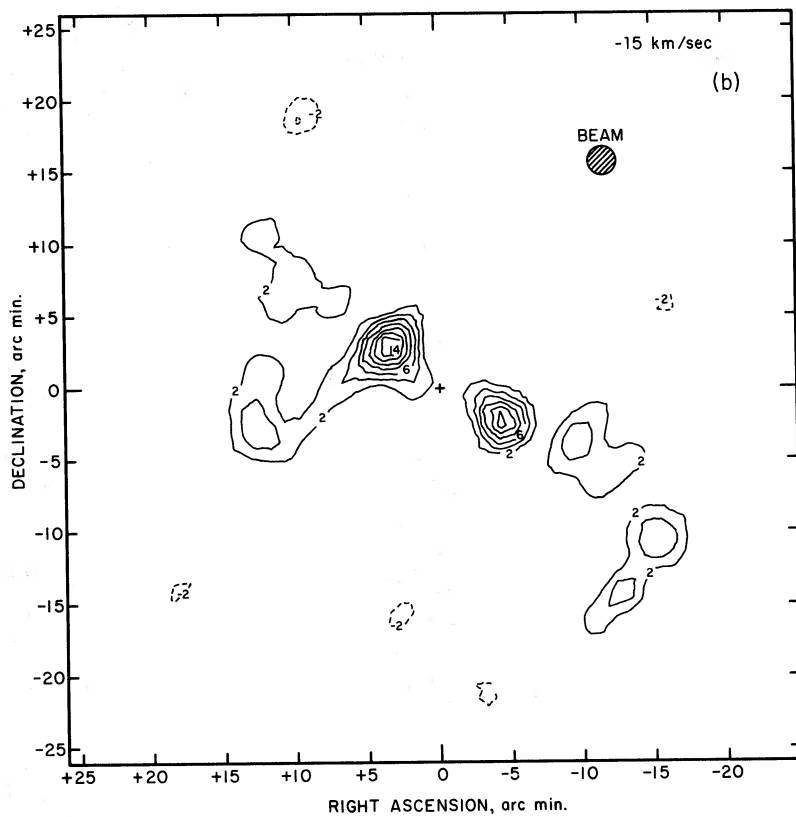


FIG. 1b

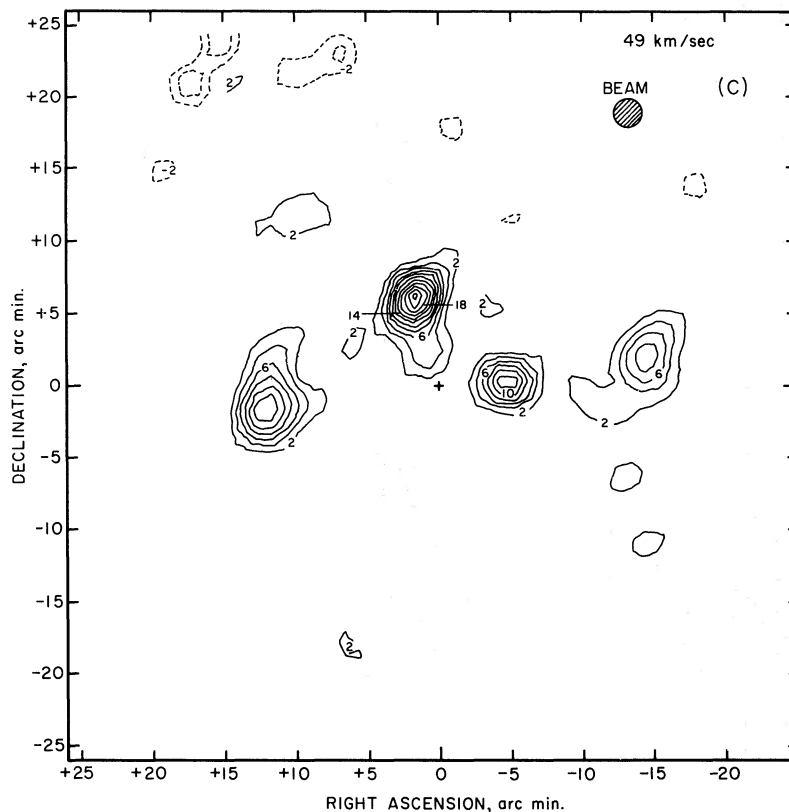


FIG. 1c

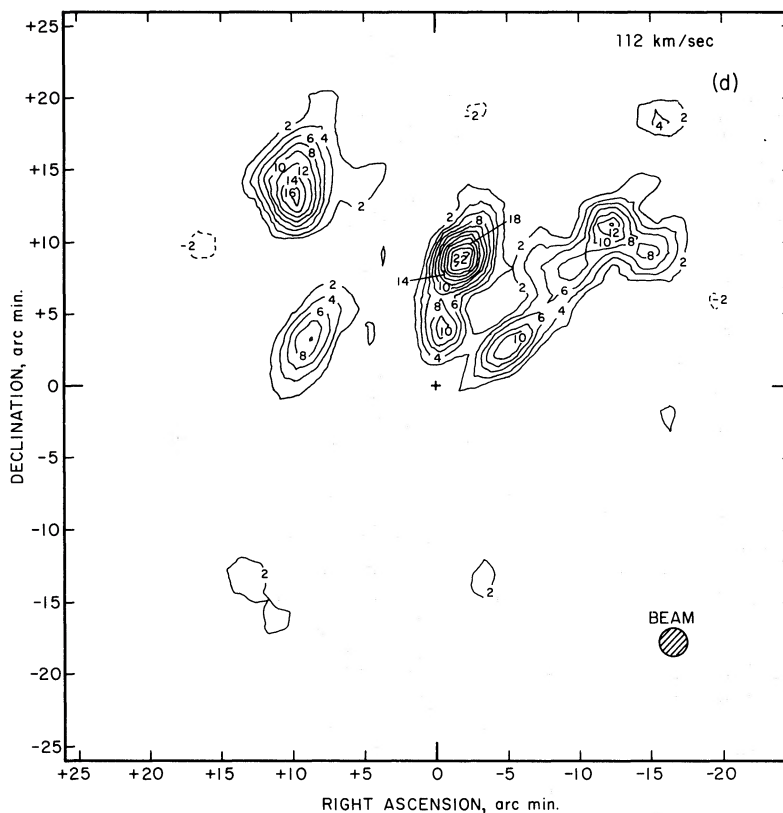


FIG. 1d

FIG. 1.—Single-channel maps of H I in M81 at velocities of (a)  $-99 \text{ km s}^{-1}$ , (b)  $-15 \text{ km s}^{-1}$ , (c)  $49 \text{ km s}^{-1}$ , and (d)  $112 \text{ km s}^{-1}$ . The bandwidth is  $21 \text{ km s}$ . The velocities are relative to the Sun. The coordinate system is taken with respect to the optical position for the center given by Gallouet *et al.* (1973), marked with a +. The contour interval is every  $2^\circ \text{ K}$  in brightness temperature. The rms noise level is  $\sim 0.4^\circ \text{ K}$  in the center of the maps, and  $0.8^\circ \text{ K}$  at  $17'$  from the center.

M81. All 23 channels, covering velocities from  $-268 \text{ km s}^{-1}$  to  $+197 \text{ km s}^{-1}$ , showed detectable signals. In the analysis program the complex visibility of any continuum emission was estimated from the broad-band channel and subtracted from the visibility of each line channel. These corrected data were then Fourier transformed to provide brightness-temperature maps of nominal neutral-hydrogen emission as observed in a  $21 \text{ km s}^{-1}$  bandwidth. The broad-band channel was also inverted to provide a map of the continuum emission from M81. The inversion and correction procedure followed was that of Rogstad and Shostak (1971). Unfortunately, the neutral-hydrogen emission seriously contaminates the broad-band continuum channel. The effects will be to make parts of the continuum map too "hot" and the corresponding positions on the neutral-hydrogen maps too "cool." The correction applied to the maps was equal to

$$\Delta T(x, y)_{\text{corr}} = \frac{\int T_L(x, y) dv}{\Delta V_{\text{con}}},$$

where  $T_L$  is the brightness temperature on the narrow-band maps, and  $\Delta V_{\text{con}}$  is the continuum channel bandwidth. The integration is performed over all line channels. The largest correction applied was about  $1^\circ \text{ K}$  and is not in error by more than  $0.2^\circ \text{ K}$  at the most intense H I regions in M81. This uncertainty is less than the rms noise.

As the neutral-hydrogen emission is very broad in angle, serious d.c. level effects will be seen if no "zero spacing" correction is introduced. An ersatz global spectrum, as observed by a 90-foot telescope, was constructed from NRAO data kindly put at our disposal by Dr. Morton S. Roberts. We incorporated this material into our own data before they were Fourier transformed. As a final adjustment, the mean d.c. level on each map, in regions where no H I signal was found, was set equal to zero. The magnitude of this correction was small, being less than  $0.2^\circ \text{ K}$ . This zero-level correction should compensate for any inconsistencies in the OVRO and NRAO temperature scales.

The field of view synthesized in this program was  $49'$  ( $\alpha$ ) by  $50'$  ( $\delta$ ). This is larger than the half-power width of the main beam of the 90-foot telescopes ( $34'$ ) and necessitates an amplitude correction. The brightness temperature as a function of position in the synthesized field depends not only on the effective resolution ( $2'$ ) but also on a gradient across the field of view introduced by the main beam. An inverse Gaussian function was applied to the maps to correct for the decrease in sensitivity. Sources found  $24'$  from the center of the map had their intensity increased by a factor of 4. As a consequence, the rms noise, which is  $\sim 0.44^\circ \text{ K}$  at the center of the field, is equivalent to  $\sim 1.8^\circ \text{ K}$   $24'$  from the map center.

In summary, the following corrections have been made to the raw data. A zero spacing was added from data provided by Dr. M. S. Roberts, and the d.c. level of each map outside of the H I was forced to be zero.

A correction was applied for neutral-hydrogen contamination of the broad-band continuum channel and its concomitant effect on the narrow-band maps. Finally, an inverse Gaussian taper was applied to all maps to correct for the directivity of the 90-foot telescope main beams.

### III. SINGLE-CHANNEL MAPS AND THE OBSERVED NEUTRAL-HYDROGEN DISTRIBUTION

Figure 1 shows four single-channel maps after all corrections were applied to the data. As mentioned, all 23 narrow-band maps show H I emission. The extreme channels at  $+197$  and  $-268 \text{ km s}^{-1}$  show brightness temperatures of  $\sim 2^\circ \text{ K}$ . However, a maximum of  $26^\circ \text{ K}$  is measured at  $+175 \text{ km s}^{-1}$ , and several channels show temperatures of  $22^\circ \text{ K}$ . These temperatures are probably underestimates, as many of the bright features are resolved neither by the  $2'$  beam nor by the  $21 \text{ km s}^{-1}$  bandwidth.

The single-channel maps contain information about the distribution of gas in the galaxy over a narrow ( $21 \text{ km s}^{-1}$ ) velocity interval. Assuming a small optical depth,  $\int T_b dv$  is proportional to the projected surface density of the neutral-hydrogen gas. A plot of the individual map peaks will delineate the denser regions in M81. This distribution is shown in figure 2. There are several features of the general distribution which stand out clearly. There is very strong emission associated with the optically defined spiral structure of the galaxy, but no strong emission at its center. There is also a great deal of clumpy emission which apparently is not associated with the main body of M81. For instance, there is a very strong region of H I emission centered about  $12'$  following the center of M81. This emission coincides closely with the position of a dwarf irregular galaxy, DDO 66/Ho IX, which can be seen on the blue Palomar Sky Survey print.

One might expect confusion by local H I to be important, for the velocities of M81 traverse the local standard of rest. Roberts (1972) finds signals at velocities of  $-60$  to  $+30 \text{ km s}^{-1}$  confused by local H I. However, M81 is at a high latitude ( $+41^\circ$ ) where an interferometer effectively resolves out local hydrogen (Hughes, Thompson, and Colvin 1971). Also, the low-intensity features of the single-channel map at  $-15 \text{ km s}^{-1}$  (fig. 1) can be followed in velocity in a systematic fashion. Some of these features are still visible at  $49 \text{ km s}^{-1}$  and/or at  $-99 \text{ km s}^{-1}$  (see fig. 1). Also, absorption effects by local gas are unlikely to be important, for the nearby radio source 3C 231 shows less than 3 percent absorption in a  $21 \text{ km s}^{-1}$  bandwidth over the appropriate velocity. Moreover, many of these "extraneous" features are found at large positive velocities, making it unlikely that local confusion is their cause.

Stochastic effects may be important, for the main-beam taper reduces the signal-to-noise ratio at the edge of the field of view. Therefore, in figure 2 we have shown map peaks only if their brightness was at least  $4^\circ \text{ K}$ . The vast majority of points fall within the  $34'$  diameter circle defining the half-power beamwidth of

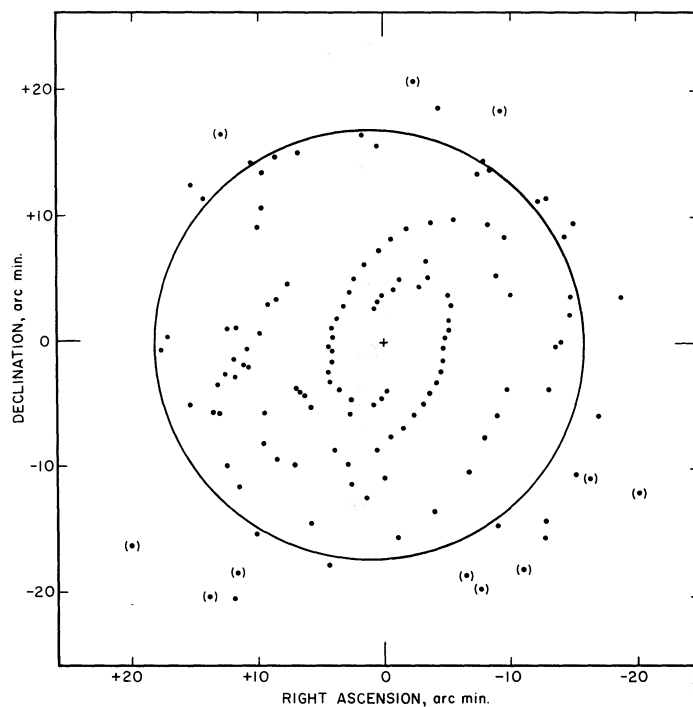


FIG. 2.—The distribution of single-channel map peaks. The full circle represents the half-power beamwidth of the 90-foot interferometer elements. The optical center of the galaxy is marked with a +. Peaks showing a signal-to-noise ratio less than 4 are in parentheses.

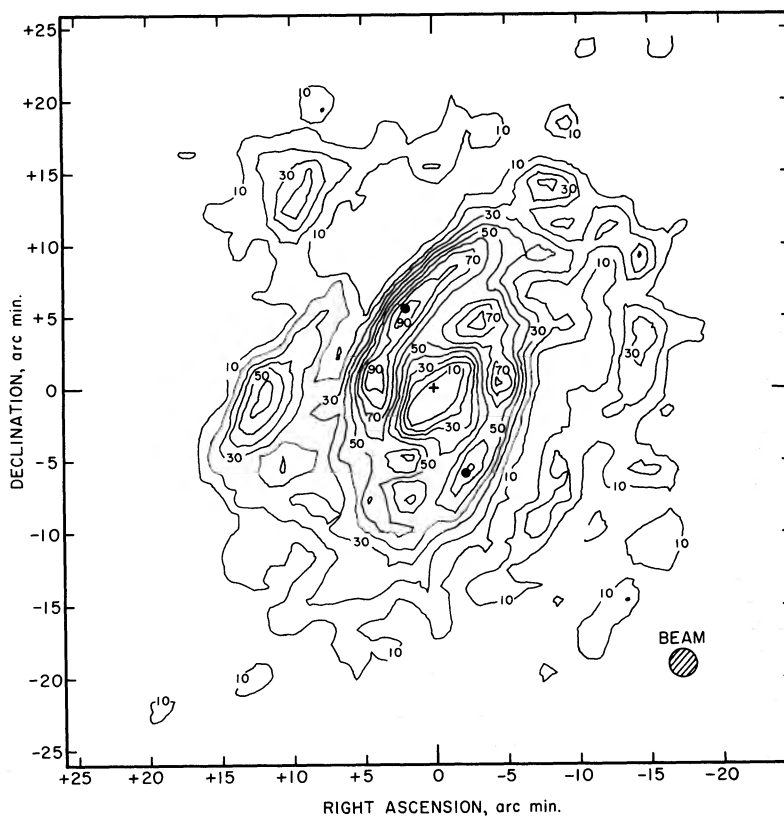


FIG. 3.—The projected column density of the neutral hydrogen on the sky. The contour units are in percent of the peak value, which is  $2.7 \times 10^{21} \text{ cm}^{-2}$  projected on the sky. The optical center of M81 is indicated with a +. The positions at which the non-circular motions caused by a density wave perturbation were calculated (see § VII) are indicated with a ●.

the 90-foot telescopes. These points, therefore, have a signal-to-noise ratio of at least 4 whereas  $4^\circ$  K points outside this circle, in extreme cases, may have a signal-to-noise ratio as low as 2.

A second mode of examining the H I distribution is to consider the beam-smoothed column density of the gas projected on the sky. This is obtained directly from the area under the line profile,  $\int T_B dv$ , provided the optical depth of the gas is small. This distribution is shown in figure 3. In figure 4 it is superposed on a blue-sensitive photograph. The integration was performed over spectral features for which  $T_B > 1.5^\circ$  K. The peak surface density on the map is  $2.7 \times 10^{21} \text{ cm}^{-2}$ , which corresponds to  $1.4 \times 10^{21} \text{ cm}^{-2}$  in the plane of the galaxy. In the central region of the map, the rms uncertainty is  $\sim 8.6 \times 10^{19} \text{ cm}^{-2}$ . Thus, the  $3\sigma$  confidence level is about the 10 percent contour. However,  $17'$  from the map center, the same confidence level is at the 20 percent contour. Hence, most of the low-level features seen on the map are real. As in figure 2, the spiral structure of the galaxy stands out remarkably. To the east of M81 there is a strong "satellite" feature, and also to the north and west of the main body of M81 there appear to be many isolated features, none of which alone are as massive as this eastern object.

Another conspicuous feature on the map is the strong depression at the center of the galaxy. The central column density is not greater than  $3 \times 10^{20} \text{ cm}^{-2}$ , very close to the  $3\sigma$  level as discussed above. The density of the minimum is thus less than 10 percent of the peak and, in this respect, this central deficiency is very similar to that seen in M31 with similar linear resolution. Guibert (1974) finds the central depression in M31 (an Sb system) to be less than 15 percent of the maximum H I column density observed. Weliachew and Gottesman (1973) have discussed possible explanations for this effect.

The total neutral-hydrogen mass observed in this survey may be calculated from a global profile which we show in figure 5. In order to create this profile, the total neutral-hydrogen flux density was calculated for each map only where  $T_B \geq 1^\circ$  K. In terms of the distance  $D$ , the integral of the profile yields a neutral hydrogen mass of

$$M_{\text{H I}}/M_\odot = 6.0 \times 10^8 D^2 \text{ (Mpc)}.$$

This result should not be an underestimate for we have included a zero-spacing measurement. However, the maximum hydrogen mass detected by this survey was calculated by integrating without regard to a temperature limit. This yields

$$M_{\text{H I}}/M_\odot = 8.1 \times 10^8 D^2 \text{ (Mpc)}.$$

Therefore, at a distance of 3.25 Mpc the neutral-hydrogen mass lies within the range

$$M_{\text{H I}}/M_\odot = (6.3\text{--}8.5) \times 10^9.$$

For the sake of simplicity in the rest of this paper, we will adopt the average of these two numbers:

$$M_{\text{H I}}/M_\odot = 7.4 \times 10^9.$$

Volders and Högbom (1961) measured a hydrogen mass for the whole system of about  $2.1 \times 10^9 M_\odot$  (distance adjusted). Their measurement was tapered by a  $36'$  half-power beamwidth. Such a taper would reduce our total H I mass of  $7.4$  to  $10^9 M_\odot$  to  $\sim 4.2 \times 10^9 M_\odot$ . However, these authors admit that they had a very low signal-to-noise ratio.

We have previously mentioned the patchy nature of the H I emission that is observed. We will see in § VIII that the dynamics of this satellite material are grossly noncircular. We feel, therefore, that most of these objects are not directly related to the main body of M81. In figure 6 we show a right-ascension cut close to the peak of the east satellite feature. It is clear that this feature is well resolved from M81, although there is a low-level halo or interconnecting bridge present. Therefore, it may be subtracted out from the general distribution of H I (fig. 3). The same may be said of the material north and west of M81. All the satellite material accounts for one-third of the total H I observed. Hence, we feel that a more sensible estimate of the total H I pertaining only to the disk of M81 is

$$M_{\text{H I}}/M_\odot = 4.9 \times 10^9.$$

The mass of H I associated with DDO 66/Ho IX is not greater than 12 percent of the total H I observed. This mass is clearly dependent upon the way the satellite is separated from M81, and the range of the H I mass is  $(0.4\text{--}0.9) \times 10^9 M_\odot$ . Figure 7 illustrates how the optical nebulosity lies relative to the H I peaks and to the feature's 30 percent H I contour. H I emission from this companion has been observed clearly from  $-57 \text{ km s}^{-1}$  to  $+154 \text{ km s}^{-1}$ .

A ringlike clumpy feature is seen in figure 3. It merges into M81 and DDO 66/Ho IX north following the center of M81, and then crosses the major axis about  $16'$  north of the center. This object can be identified with the ring of optical emission first detected by Arp (1965). Figure 7 shows a representation of the ring relative to the H I peaks. It is clear that the optical emission of the ring is much less patchy (see the cover of *Science*, 1965 April 16) than is the H I emission. The most intense components of this feature,  $T_B \approx 14^\circ\text{--}16^\circ$  K, are at a velocity of  $+112 \text{ km s}^{-1}$ . Figure 1 shows several regions associated with this object. The eastern segment of the ring contains  $\sim 50$  percent of the H I mass of the feature. The total hydrogen mass of the ring is 16 percent of all the H I observed or  $\sim 1.2 \times 10^9 M_\odot$ . We will show in § VIII that the gas dynamics of the ring are grossly noncircular for that projected position in M81. We presume, therefore, that the object is unlikely to be in the plane of that galaxy.

There are several weak objects preceding M81 which we have not discussed. The total H I mass concerned is about 6 percent of the H I observed. We are describing patchy features whose individual gas mass is  $5 \times 10^6\text{--}1 \times 10^8 M_\odot$ . This may represent part of the halo surrounding M81, M82, and NGC 3077 found by Roberts (1972). Or, alternatively, this material may be

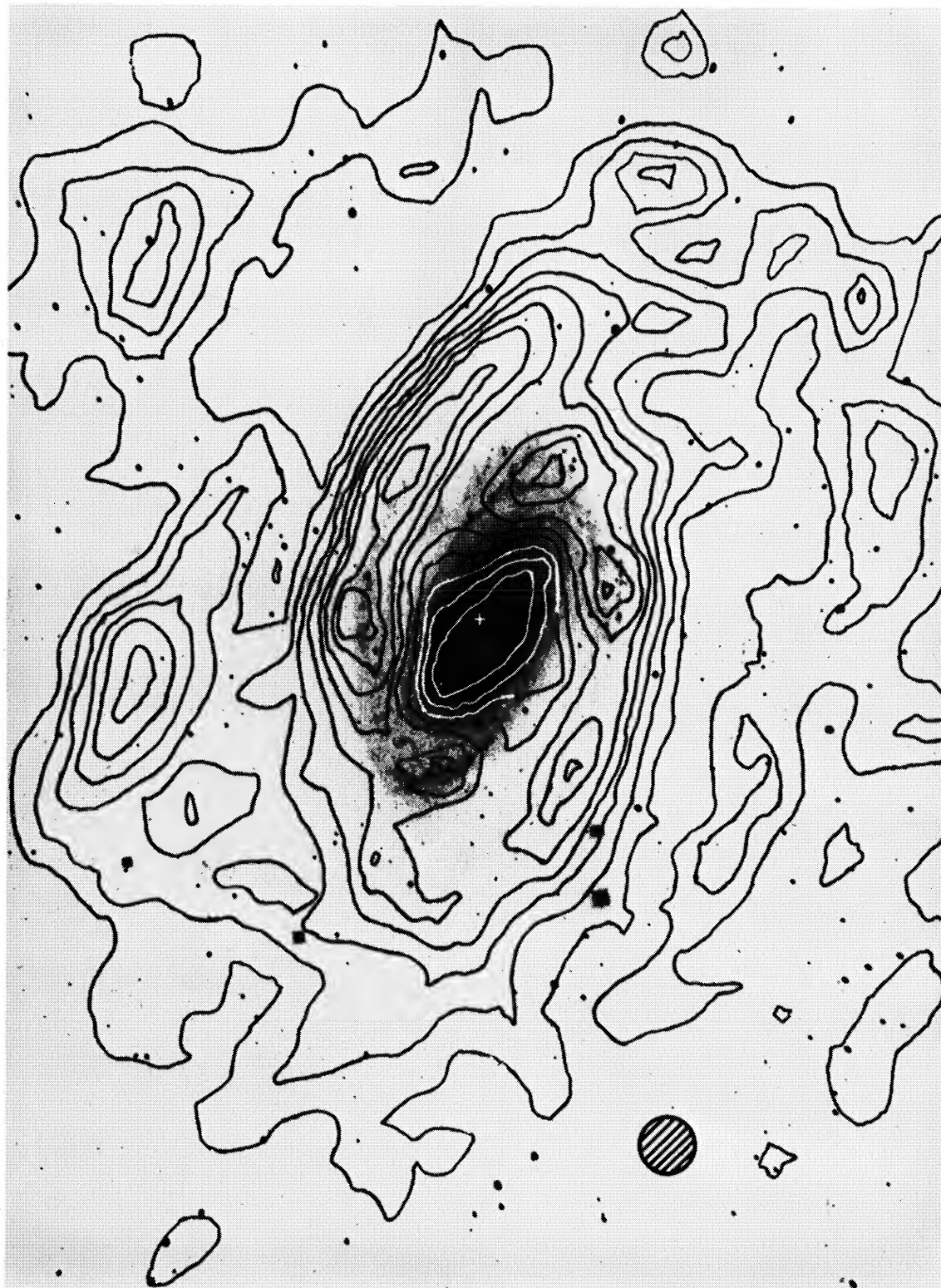


FIG. 4.—The contours of equal H I density of fig. 3 superposed on a photograph of M81 (courtesy Dr. A. G. Smith)



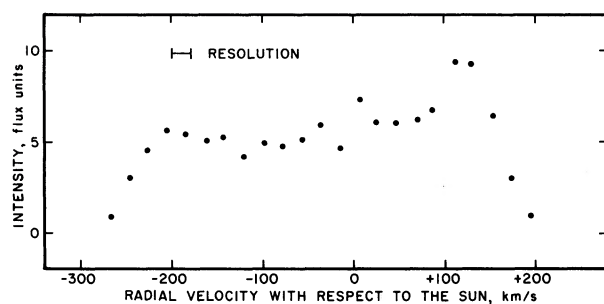


FIG. 5.—A global velocity profile constructed from the single-channel maps. The instrumental resolution is  $21 \text{ km s}^{-1}$ .

associated with the spiral structure of the galaxy. We will discuss these features in more detail in §§ VII and VIII.

#### IV. THE OBSERVED KINEMATICS OF M81

By calculating the mean velocity of spectra (profile center of gravity) at each position in M81, we may determine a representative radial velocity. In figure 8 we display the distribution of mean velocities across the synthesized field of view. In figure 9 this distribution is compared with a blue-sensitive photograph. The mean spectral value was calculated only if the line power was greater than  $4\sigma$  ( $\sim 190^\circ \text{ K km s}^{-1}$ ) and if the profile temperature was greater than  $1.5^\circ \text{ K}$ . These signal-to-noise criteria are responsible for the gap in the center of the velocity map. This distribution does not reveal the intrinsic dynamics of the H I in M81 due to our finite resolution. The velocity seen at any point in the galaxy is weighted by the density distribution of the gas within the synthesized beam. The map reveals many small-scale “wiggles” on the isovelocity

contours, particularly where the spiral arms are well resolved to the north of the galaxy. These wiggles could be caused by streaming motions associated with the spiral structure (Lin, Yuan, and Shu 1969), and we will discuss this possibility in § VII. Here we will confine our attention to the more obvious kinematical effects.

The velocity observed at any point in the galaxy is the sum of rotational and line-of-sight noncircular terms:

$$V_{\text{obs}} = V_{\text{rot}}(R) \cos \theta \sin I + V_{\text{nc}}(R, \theta) + V_{\text{sys}}, \quad (1)$$

where  $R$  is the radius in the plane of the galaxy at some point,  $\theta$  is the azimuth angle in the galactic plane relative to the major axis, and  $I$  is the inclination angle.  $V_{\text{nc}}$  represents any noncircular term, and  $V_{\text{sys}}$  is the recessional or systemic velocity of the galaxy.

It is clear from the form of the rotational term that circular dynamics imply a symmetry about the major axis and reflected through the center of the galaxy. Any deviations from circular symmetry in the dynamics and/or in the distribution of the neutral hydrogen will affect the observed line-of-sight velocity pattern. Thus DDO 66/Ho IX, which is a dwarf irregular system east of M81, is clearly not at the expected circular velocity for material in the plane of M81. For instance, the  $0 \text{ km s}^{-1}$  isovelocity contour cannot be reproduced by simple circular velocity models. We will also show that the Arp feature is not at its expected circular velocity. Fortunately, these features are separated well enough from the apparent major axis of M81 that the principal geometric and kinematic parameters of the galaxy can be determined with certainty. Before we can quantitatively investigate the noncircular nature of any features, we must determine the major-axis position angle, the inclination of the galaxy, and the systemic velocity. Unlike M51, for example (Weliachew and

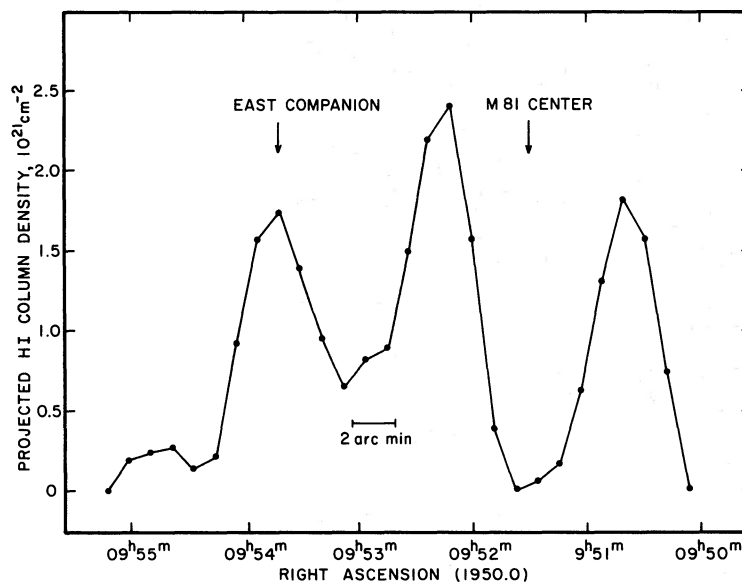


FIG. 6.—A right ascension cut through the data in fig. 4. The declination of the cut is  $\delta = 69^\circ 17' 57''$ . The angular resolution is  $2'$ .

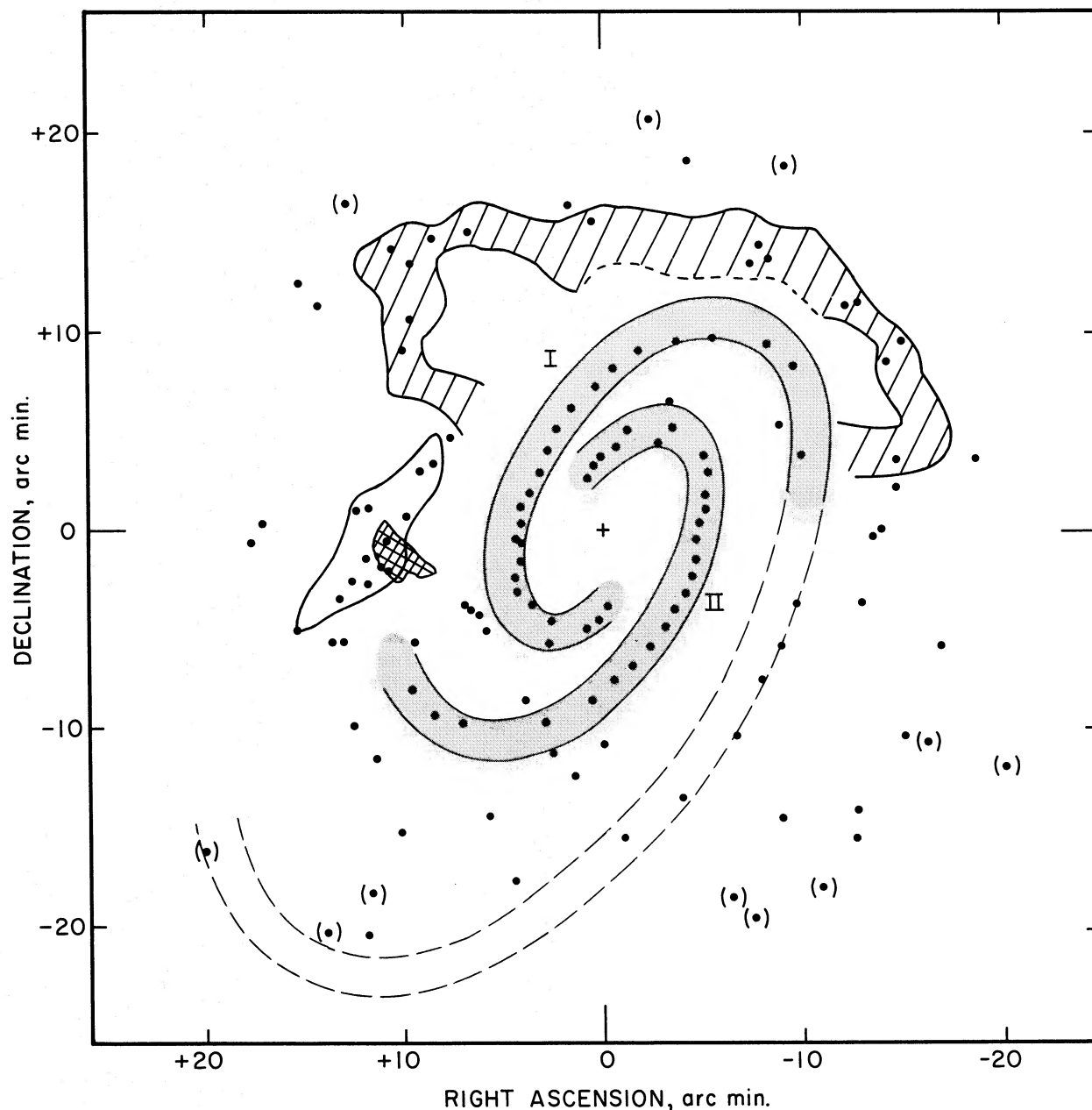


FIG. 7.—The distribution of single-channel neutral H I peaks compared with several features discussed in the text. The stippled feature represents spiral arms, I and II, of M81 with a pitch angle  $\mu = 77^\circ$ . The less certain extension of arm I has been marked with a dashed line. The single crosshatched region shows the Arp ring feature. The double crosshatched region marks the nebulosity of DDO 66/Ho IX. This feature coincides well with the hydrogen east companion, which is outlined by the 30% contour of fig. 3.

Gottesman 1973), there are no great morphological asymmetries; the optical emission, the H I distribution and the H I kinematics all indicate the same major-axis position angle. The optically determined values range from  $147^\circ$  (Danver 1942; Brandt, Kalinowski, and Rosen 1972) to  $149^\circ$  (Boggess 1959). Using the data in figure 8, our value is determined to be  $151^\circ \pm 2^\circ$ .

The systemic velocity was obtained from symmetry considerations. Spectra along the major axis  $4' < |R| < 20'$  were symmetrized. The resulting systemic velocity is  $V_{\text{sys}} = -31 \pm 6 \text{ km s}^{-1}$ . This is probably the best value we may determine from our data, as the signal-to-noise ratio is very low in the central region of the galaxy and noncircular velocities confuse the single channel maps. The single-channel map, where

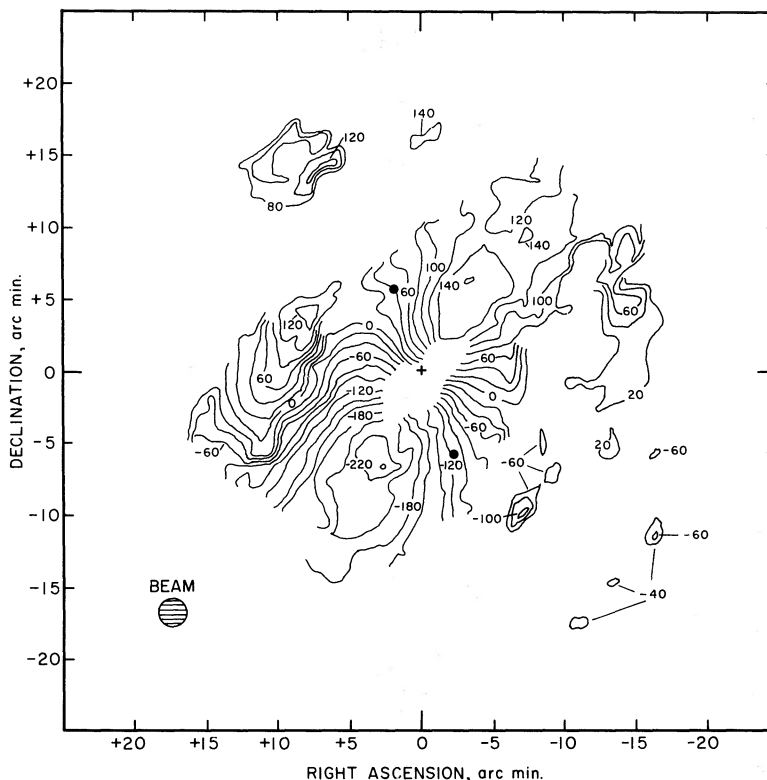


FIG. 8.—The observed mean spectral velocity in M81. The velocity resolution is  $21 \text{ km s}^{-1}$ . The optical center of the galaxy is indicated by +. The contour units are every  $20 \text{ km s}^{-1}$  relative to the Sun. The positions at which the noncircular motions generated by a density-wave perturbation were calculated (see § VII) are indicated with a ●.

$V_{\text{rot}} = 0$ , cannot be located reliably. The optical value given in the *Reference Catalogue* (de Vaucouleurs and de Vaucouleurs 1964) is  $-44 \text{ km s}^{-1}$ .

The inclination angle of the galaxy, defined as the angle between the projected plane on the sky and the plane of the galaxy, can now be determined. In the absence of noncircular terms, the inclination and rotation velocity are related at any position  $(R, \theta)$  in the galaxy by

$$V(R)_{\text{rot}} = \frac{|[V(R)_{\text{obs}} - V_{\text{sys}}]|}{\cos \theta \sin I}.$$

The radius  $R$  in the plane of the galaxy is also a function of  $I$ . Thus, by a least-squares technique, we can find an  $I$  such that the spread of the calculated values of  $V(R)_{\text{rot}}$  is minimized. We attempted to reduce the influence of expansion or contraction velocities by choosing points close to the major axis. By this technique  $I$  was determined to be  $58 \pm 3^\circ$ . Connolly *et al.* also found this value by geometrical arguments. The optical position given by Gallouet *et al.* (1973) was used as a reference point throughout the reduction of the data discussed in this paper. However, a more precise position has been published by van der Kruit (1974) ( $\alpha = 09^{\text{h}}51^{\text{m}}27^{\text{s}}.2$ ,  $\delta = +69^\circ 18' 08''.3$ ). Within the errors of our data there is no disagreement with this position.

In the next section we quantitatively investigate the dynamics of the galaxy.

#### V. MODEL CALCULATIONS AND RESULTS

The model calculations we are about to describe investigate large-scale phenomena and make no attempt to describe dynamical terms due to spiral structure. The method we have used is the same as that employed in our study of M51. We have corrected the gas distribution for the effects of finite resolution following the method of Bracewell and Roberts (1954). The data in figure 3 were corrected for a  $2'$  half-power Gaussian beam. After each iteration, negative values were set to zero and five iterations were performed. The kinematics were approximated by the equation for which Brandt and Scheer (1965) have tabulated various dynamically related functions. The rotational velocity at a radius  $R$  is

$$V(R)_{\text{rot}} = \frac{V_{\text{max}} R/R_{\text{max}}}{[\frac{1}{3} + \frac{2}{3}(R/R_{\text{max}})^n]^{3/2n}}, \quad (2)$$

where  $V_{\text{max}}$  is the maximum rotation velocity observed at a radius  $R_{\text{max}}$  and  $n$  is a shape parameter. The parameter  $n$  determines how fast the curve rises to  $V_{\text{max}}$  for  $R < R_{\text{max}}$  and how fast it falls from  $V_{\text{max}}$  for  $R > R_{\text{max}}$ . In the case where  $n$  is small, the rotation curve

risers quickly to  $V_{\max}$ , but thereafter falls very slowly. The deconvolved H I distribution was combined with a model velocity function and a weighting function appropriate for a 2' Gaussian beam. In this fashion a theoretical isovelocity map was computed and compared with the observed map. In figure 10 we make such a comparison with a Brandt velocity model for which no noncircular terms were employed. This is the best model in terms of circularly symmetric velocities over the whole galaxy. The Brandt parameters used were

$$R_{\max} = 5.7, \quad n = 4.75, \quad V_{\max} = 253 \text{ km s}^{-1}.$$

(All models investigated employed an inclination angle of  $58^\circ$  and a major-axis position angle of  $151^\circ$ .) The following conclusions may be drawn: (1) The kinematics of the east companion DDO 66/Ho IX are grossly noncircular. The peak of the companion is moving at a velocity such that  $(V_{\text{obs}} - V_{\text{model}}) \simeq +120 \text{ km s}^{-1}$ . (2) The strong north-following emission associated with the Arp ring feature also shows a large deviation from circular velocities,  $(V_{\text{obs}} - V_{\text{model}}) \simeq 100 \text{ km s}^{-1}$ . (3)  $R_{\max}$  is not observed to be the same in the northern and southern halves of the galaxy.

Furthermore, in the south, only the western quadrant appears to follow expected circular dynamics. In the north, noncircular velocities are seen on the north-preceding corner and in regions associated with the Arp ring. Otherwise the observed dynamics closely follow circular expectations. The extended spiral-arm material and other satellite features west of M81 show projected noncircular terms of less than  $50 \text{ km s}^{-1}$ . It can be seen, therefore, that the dynamics of the north and south must be examined separately. The best circular solution, for the two halves of the galaxy, is given in table 1. The errors are conservative estimates obtained by varying one parameter in the model calculation while holding the other two constant. The quoted error was determined from the value which doubled the sum of  $(V_{\text{obs}} - V_{\text{model}})^2$ . The differences observed in the north and the south for  $R_{\max}$  and  $n$  are significant but not unusual. Such differences in the apparent circular velocity are known in our Galaxy (Kerr 1969) and in M31 (Gottesman and Davies 1970), and it is possible that similar asymmetries were detected in our previous study of M51. Such differences must be indicative of noncircular effects either in the gravitational forces determining the rotational motions (e.g., large-scale mass asymmetries) or, more likely, systematic nonplanar motions. Optical rotation data

is very scanty, but we compare the H II velocities (Münch 1959, corrected for our geometrical parameters) with our rotation curves in figure 11. Our rotation data are in general agreement with the rotation curve presented by Roberts and Rots (1973).

The velocities on the south-following quadrant are extremely noncircular, and are clearly related to the presence of the east satellite. We were therefore interested in seeing whether this was a confusion phenomenon or whether the plane of M81 had been distorted due to an interaction with DDO 66/Ho IX. The H I peak of this object is  $\alpha = 09^{\text{h}}53^{\text{m}}44^{\text{s}}$ ,  $\delta = 69^\circ 17' 30''$ , and the major-axis position angle is  $146^\circ$ . We therefore investigated the spectra along the minor axis (position angle  $= +56^\circ$ ) of the companion. An axis-velocity diagram is presented in figure 12. Strong emission from the satellite feature is seen along its minor axis out to 2' northeast and 3.5 southwest. Low spectral wings extend out to 7' northeast and 10' southwest of the H I peak of DDO 66/Ho IX. We also show on the diagram a comparison of the mean velocity expected from purely circular dynamics in M81 and the measured mean spectral velocity. It is seen that discrepancies start becoming significant around 6' southwest of the H I peak of the companion. Part of this effect is undoubtedly due to the spectral feature associated with the companion. However, as we get closer to the satellite there is no M81 emission seen near the expected velocities. Four arc minutes from the companion, the velocity discrepancy is  $77 \text{ km s}^{-1}$ . The spectra of M81 and the companion merge at about 3' from the companion. It would appear, therefore, that a small fraction of the noncircular effect is due to confusion; the major effect is genuine noncircular motion in M81.

From the velocity data (fig. 8), the southern half of M81 is approaching us. Hubble (1943) and Simkin (1967) have investigated the reddening within that galaxy and have concluded that the southwest edge of the system is nearest the observer. These two pieces of information imply that the arms of M81 are trailing. Thus the noncircular motions at the southeast edge of M81 could be explained either by expansion in the plane of the galaxy or by relative motion in M81 away from us along the line of sight. If, indeed, the latter explanation is correct, then the fact that DDO 66/Ho IX is redshifted relative to M81 implies that it is behind the plane of that galaxy.

## VI. THE MASS OF M81

Having determined a circular velocity model for the galaxy, we may calculate the mass of the system. The total mass is not calculated reliably as it depends on an extrapolation to infinitely large radii, well beyond the limit of the observations. We may use the Brandt and Scheer tables to calculate the mass contained in a cylinder of given radius perpendicular to the plane. The Arp ring feature confuses observations along the northern semimajor axis  $\sim 16'$  from the center; but in the south, measurements exist beyond 20' from the

TABLE 1  
BRANDT ROTATION FUNCTION PARAMETERS  
FOR THE GALAXY M81

	North	South	Error
$R_{\max}$ .....	5.0	6.4	$\pm 0.4$
$n$ .....	3.5	6.0	$\pm 0.4$
$V_{\max}$ (km s $^{-1}$ ).....	250	256	$\pm 8$

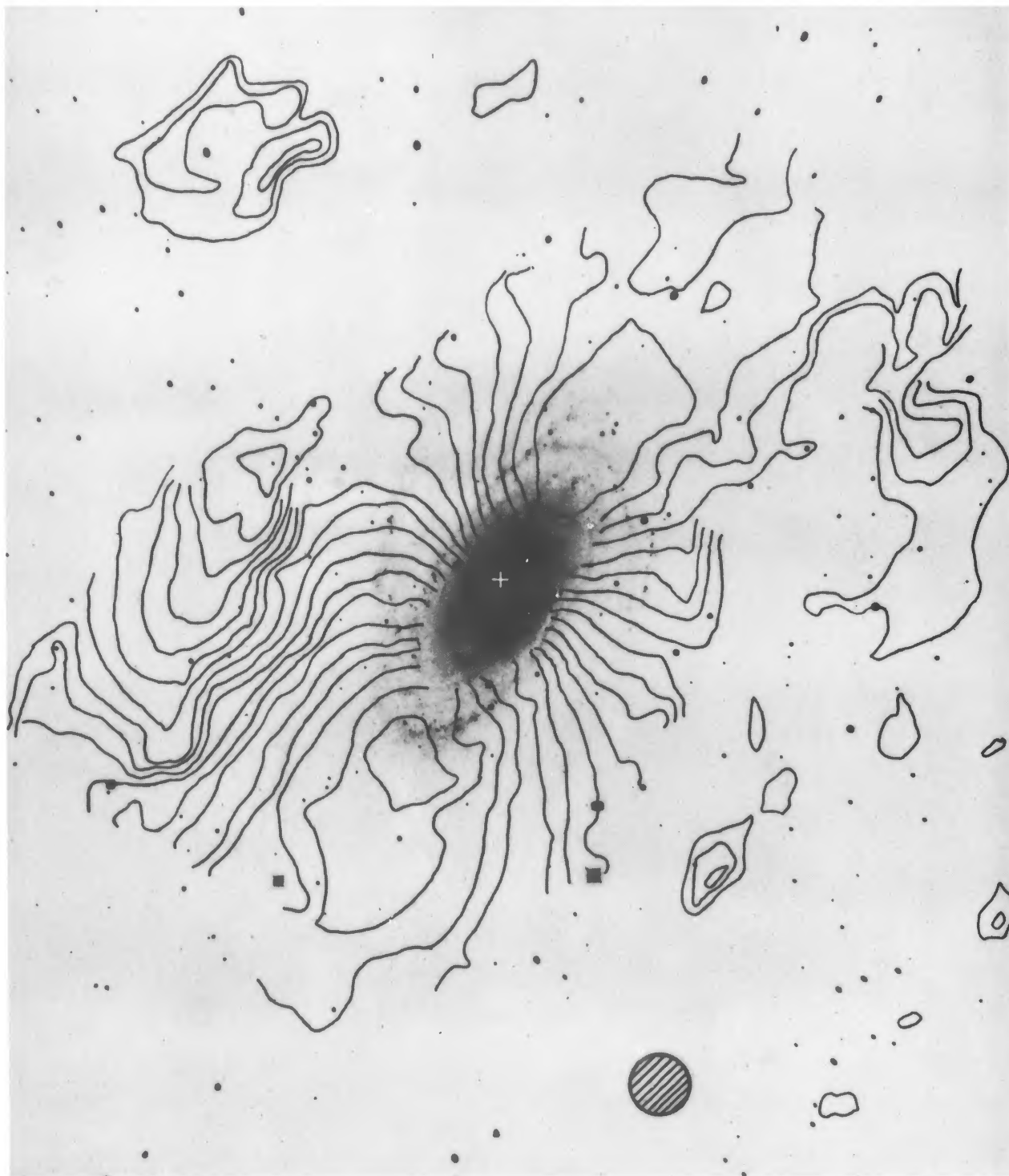


FIG. 9.—The isovelocity contours of fig. 8 superposed on a blue-sensitive photograph of M81 (courtesy Dr. A. G. Smith)



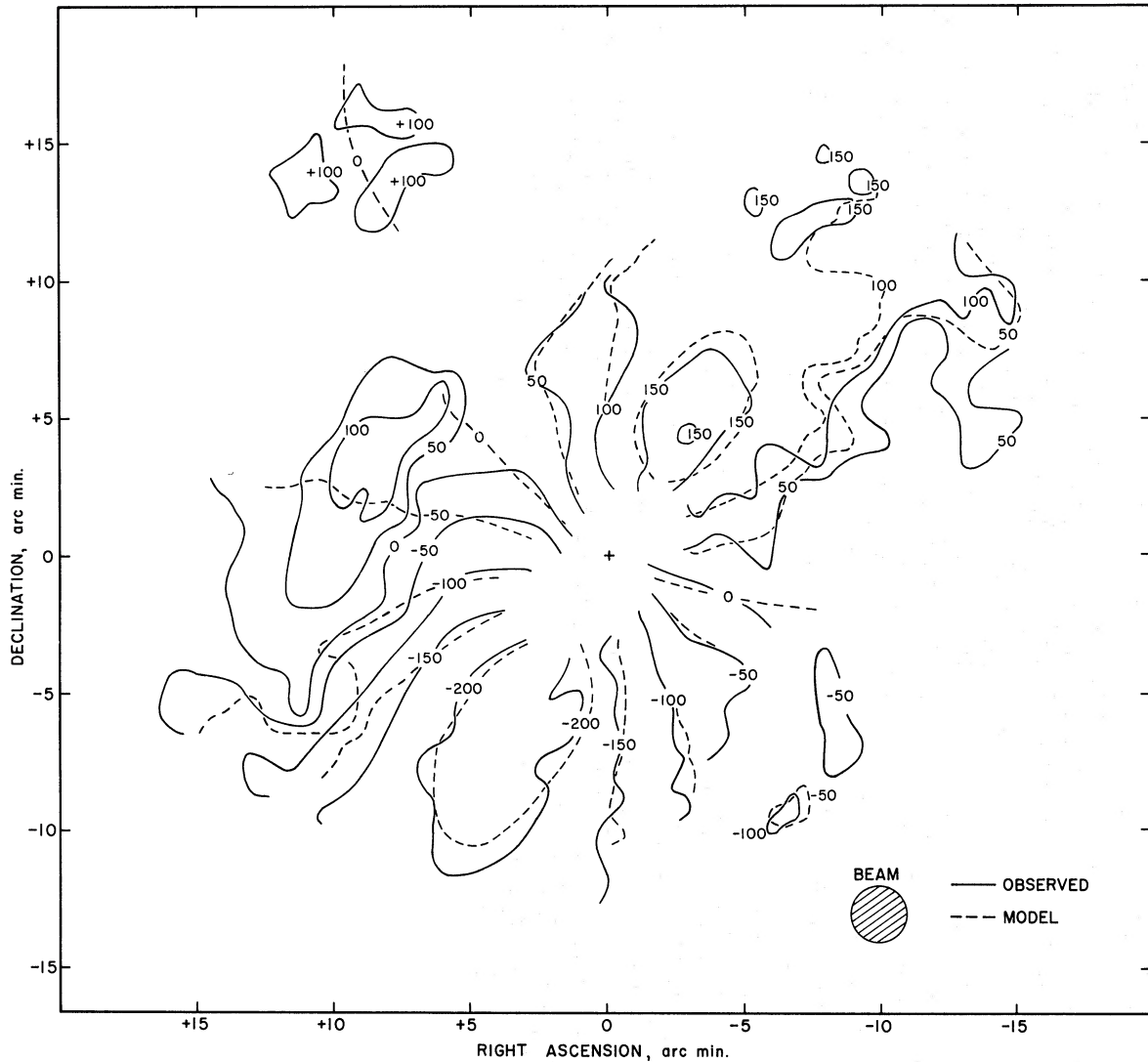


FIG. 10.—A comparison of the observed mean line-of-sight spectral velocities with that predicted from a circularly symmetric velocity model based on a Brandt rotation law. (This is not the best model found in this study; see § V.)

center. Considering off-axis measurements as well, we believe that a mass inside a radius of 20 kpc can be calculated safely. After including a correction for finite thickness of the disk ( $c/a = 0.2$ ), we find in the north  $M(20) = 1.0 \times 10^{11} M_{\odot}$ , while in the south  $M(20) = 1.2 \times 10^{11} M_{\odot}$ . We will adopt the mean value for the bounded mass. Within 20 kpc Roberts and Rots (1973) find  $(1.0-1.3) \times 10^{11} M_{\odot}$ . The blue luminosity,  $L_B$ , may be obtained from the data of Brandt *et al.* (1972). However, their data must be corrected for obscuration by our Galaxy (0.07 mag, according to Sandage 1973) and obscuration internal to M81 (0.8 mag, according to Holmberg 1958). The corrected blue luminosity is  $2.2 \times 10^{10} L_{\odot}$ . We have derived an H I mass for this galaxy of  $4.9 \times 10^9 M_{\odot}$ . Thus, we may calculate the standard ratios of interest

$M_{\text{H I}}/M(20)$ ,  $M_{\text{H I}}/L_B$ , and  $M(20)/L_B$ . These are listed in table 2.

We may also compare the mass surface density with the surface brightness as a function of radius, which is done in figure 13. We have corrected the Brandt *et al.* values to face-on luminosities. Over a very wide range in radius, from 2 kpc to 9 kpc, the ratio  $M(R)/L(R)$  is fairly constant at a value of about 13 or 12, if corrected only for obscuration in our Galaxy. Almost identical  $M(R)/L(R)$  values were found in M31 (Gottesman and Davies 1970) for the disk region. No corrections were applied for obscuration internal to either galaxy. However, in the case of M81 this correction is a factor of 2.1 for the integrated luminosity. As a reference, the most widely accepted value in the solar neighborhood is  $M/L \sim 3.8$  (Oort 1965). Interestingly, the value of



TABLE 2  
PARAMETERS OF M81

Optical position of center.....	$\alpha_{1950.0} = 9^{\text{h}}51^{\text{m}}27^{\text{s}}$	
Radio (H I) position of center.....	$\delta_{1950.0} = 69^{\circ}18'08''$	
	$\alpha_{1950.0} = 9^{\text{h}}51^{\text{m}}27^{\text{s}} \pm 4^{\text{s}}$	
	$\delta_{1950.0} = 69^{\circ}17'50'' \pm 20''$	
Systemic velocity (with respect to the Sun).....	$-31 \pm 6 \text{ km s}^{-1}$	
Distance (adopted).....	3.25 Mpc	
Major-axis position angle.....	$151^{\circ} \pm 2^{\circ}$	
Inclination.....	$58^{\circ} \pm 3^{\circ}$	
Mass of neutral hydrogen.....	$4.9 \times 10^9 M_{\odot}$	
Total luminosity $L_B^0$ (corrected, see § VI).....	$2.2 \times 10^{10} L_{\odot}$	
	Northwest	Southeast
Maximum rotation velocity.....	$250 \pm 8 \text{ km s}^{-1}$	$256 \pm 8 \text{ km s}^{-1}$
Radius of maximum velocity.....	$4.75 \pm 0.4 \text{ kpc}$	$6.1 \pm 0.4 \text{ kpc}$
Brandt shape parameter.....	$3.5 \pm 0.4$	$6.0 \pm 0.4$
Mass within 20 kpc $M(20)$ .....	$1.0 \times 10^{11} M_{\odot}$	$1.2 \times 10^{11} M_{\odot}$
Adopted mass $M(20)$ .....	$1.1 \times 10^{11} M_{\odot}$	
$M_{\text{HI}}/M(20)$ .....	0.044	
$M_{\text{HI}}/L_B^0$ .....	0.22	
$M(20)/L_B^0$ .....	5.	

## VII. THE SPIRAL STRUCTURE OF M81

### a) The Morphology

The high-density material defining the spiral arms of M81 is just resolved in this study. If the gas in the arms seen in figure 3 has a Gaussian distribution, the intrinsic half-power width of the arms is 2.25 or  $\sim 2.1$  kpc. According to Yuan (1969), the Sagittarius

arm in the Milky Way System could be as thick as 2 kpc at some galactic radii. In regions where the arms are separated from the main body of M81, we can estimate the arm-interarm gas density contrast. (In discussing the spiral structure of M81 we will refer to arms I and II. This convention is illustrated in fig. 7.) In arm I, at a radial distance of 10 kpc in the plane of the galaxy (at position angle  $+40^{\circ}$  relative to the northern semi-major axis), the density contrast

$$\frac{\sigma_{\text{max}} + \sigma_{\text{min}}}{\sigma_{\text{max}} - \sigma_{\text{min}}} \sim 2.9;$$

while in arm II, at a radial distance of 7.5 kpc (at position angle  $+40^{\circ}$  relative to the southern semimajor axis), the contrast appears to be  $\sim 4.9$ . These density contrasts have been derived from our model calculated in § V and should be reliable since a zero-spacing observation was included in our reductions. However, taking into account the instrumental parameters and uncertainties, the maximum error in the ratios is  $\pm 35$  percent. Thus the difference between the two regions may not be very significant. These values are similar to density contrasts found in our Galaxy (Yuan 1969; Burton 1971).

The spiral structure is well defined both at optical and at H I wavelengths. We approximate the spiral in the following fashion:

$$R = R_0 \exp(\varphi \cot \mu), \quad (3)$$

where  $\mu$  is the acute angle between the radius and the tangent to the spiral,  $\varphi$  (in radians) is the phase of the spiral relative to the position angle of the semi-major axis ( $331^{\circ}$  for arm II and  $151^{\circ}$  for arm I);  $\varphi > 0$  in the direction of the opening spiral. For both arms  $R_0 = 5.8$ . Danver (1942) finds  $\mu = 81^{\circ}$  for the optical arms, and Connolly *et al.* (1972) find  $\mu = 80^{\circ}$  for the prominent dust lanes. We find that  $\mu = 77^{\circ}$  fits both the northern- and southern-arm H I peaks very

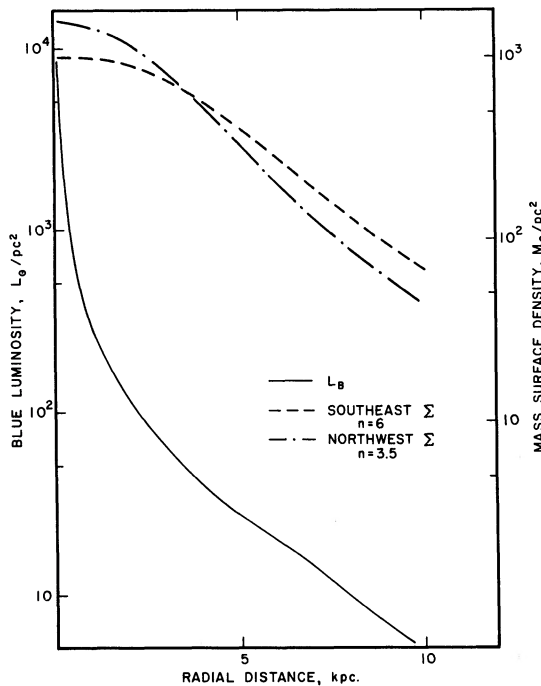


FIG. 13.—Comparison along the major axis of the face-on blue luminosity (Brandt *et al.* 1972), not corrected for obscuration, with the mass surface density,  $\Sigma$ , computed from our best fitting rotation models (§ V).

well, although there are some systematic variations. The spiral pattern is clearly delineated by the H I peaks where the optical arms can be seen. Beyond these regions, the spiral pattern becomes less well defined. In arm I, the inner part of the spiral ( $\varphi < 110^\circ$ ) is relatively tightly wound,  $\mu \approx 80^\circ$ , while the outer spiral is looser with some regions fitting a pattern with  $\mu \approx 74^\circ$ . In arm II the inner part of the spiral is looser than in arm I with  $\mu \approx 74^\circ$ , while the outer parts can be fitted better by a spiral with  $\mu$  in the range of  $77^\circ$ – $80^\circ$ . In figure 7 we have drawn a spiral with  $\mu = 77^\circ$  through the H I peaks; the width of the spiral arms is  $\sim 2$  kpc. By allowing a  $\pm 3^\circ$  variation in  $\mu$ , arms I and II can be traced clearly through more than  $180^\circ$  in  $\varphi$ . The peaks that fall between the arms might represent interarm spurs.

Much of the low-density material, including the westernmost H I clumps, may be external to M81 and have nothing to do with the ordinary structure of that galaxy. However, there is very good continuity between the stronger of these preceding features and the more obvious inner structure of arm I. Owing to its reduced certainty, we have drawn a dashed line, in figure 7, through this extended spiral material.

Brandt *et al.* (1972) claim that the optical arms can be traced to within  $3'$  of the galaxy center. The strong H I can be found within  $4'$  of the center (fig. 2). However, there is evidence for material extending to about  $1'$ – $2'$  from the center along the minor axis at velocities more positive than  $-15$  km s $^{-1}$ . This material, which appears to be associated with arm II, is clearly seen on the map at  $49$  km s $^{-1}$  in figure 1.

The spiral structure we have discussed is also shown by Rots and Shane (1974) who have presented a preliminary map of the H I in M81 obtained with a resolution of  $50''$ . The agreement between the two studies is very good. However, the observations of Rots and Shane suffer a lack of information from baselines shorter than 36 meters. Consequently they have a serious bowl-shaped zero-level effect in their data. To partially overcome this difficulty, they have used the old measurements of Volders and Högbom (1961). These authors acknowledge a ratio of two between the extreme values of their H I mass. Therefore, it is very unreliable to make use of this data as a zero spacing.

The spiral arms of M81 are well populated with H II regions (Connolly *et al.* 1972), and in figure 14 we compare the H II distribution (smoothed to  $2'$  resolution) with the H I distribution along the major axis. Both in the north and the south the H II maxima occur in regions of large H I density. However, the H I surface density does not change markedly for  $R > 5'$ , but the H II surface density drops sharply. This apparent disparity may be explained by the density-wave theory of spiral structure which we will now discuss.

#### b) The Spiral Structure as a Density Wave

Shu, Stachnik, and Yost (1971) applied the density-wave theory of spiral structure to M81. Following Lin's proposal (1970), these authors assumed that the angular speed,  $\Omega_p$ , of a spiral pattern is given by the rotation velocities close to the farthest observed H II regions. They used the velocities of H II regions

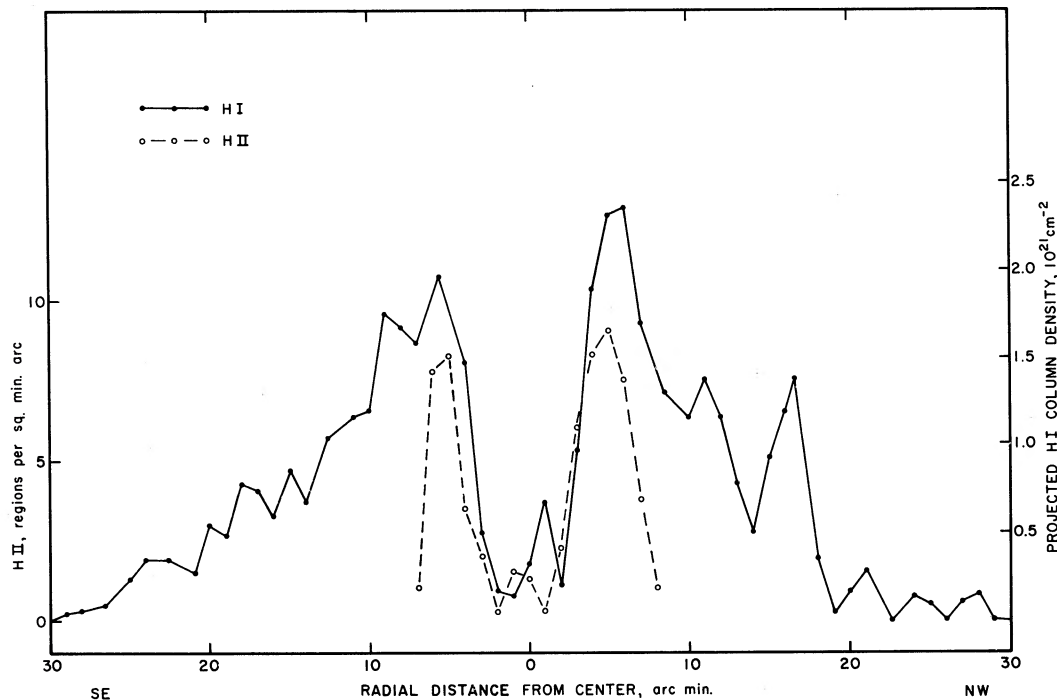


FIG. 14.—Comparison of the major axis surface density of H I (this study) and H II regions (data taken from Connolly *et al.* 1972). Both densities are projected on the sky. At a distance of 3.25 Mpc,  $10' = 9.5$  kpc.

measured by Münch (1959). Their derived pattern speed,  $\Omega_p$ , was  $17.5 \text{ km s}^{-1} \text{ kpc}^{-1}$  at the assumed distance of 3.25 Mpc. Their corotation circle was  $14'6$  (13.8 kpc) from the center, close to the farthest H II region observed by Münch at  $15'5$  (14.7 kpc). Using the dispersion relationship for linear density waves and Münch's optical data, Shu *et al.* derived a model spiral pattern that was reasonable but slightly too tight. In addition, their model predicted significant star formation to be occurring  $12'$  (11.4 kpc) from the center whereas large numbers of H II regions are not observed beyond  $8'$  (7.6 kpc) from the center. They therefore suggested an overall deficiency of interstellar gas beyond  $8'$ . However, figures 3 and 14 of the present study show a significant amount of interstellar gas  $12'$  from the center.

This contradiction has led us to redetermine the angular speed of the spiral pattern from our H I data. We have derived the frequency of the pattern from the measured radial wavelength of the spiral wave in a region where our H I results best delineate the pattern. We have estimated the radial wavelength,  $\lambda$ , of the spiral at  $8'8$  (8.4 kpc) from the center on the major axis. If the peaks of the single-channel maps (fig. 2) are assumed to define the spiral pattern, we find  $\lambda = 5.2$  kpc and  $\lambda = 5.9$  kpc along the northern and southern semimajor axes. The epicyclic frequency,  $\kappa$ , and the mass surface density were obtained from our rotational velocities. The gas surface density was obtained directly from the observations. The calculations have been made following the method of Lin *et al.* (1969) for a thin disk. (According to these authors, a finite disk thickness does not critically affect the results.) The most uncertain parameter used in calculating  $\Omega_p$  is the mass surface density,  $\sigma$ . We have made use of the errors in our kinematical model (see § V) and find  $\sigma$  to be uncertain by a factor of 1.5 in either direction. Thus we find a pattern velocity of  $18.9$  and  $18.3 \text{ km s}^{-1} \text{ kpc}^{-1}$  in the northwest and southeast, respectively, corresponding to corotation radii of  $10.5$  and  $11.4$  kpc. These are the maximum values of the corotation radius allowed by the uncertainties in our model mass distribution.

It appears, therefore, that within the accuracy of our observations the corotation radius in M81 cannot be greater than  $12'$  compared with  $14'6$  suggested by Shu *et al.* On the other hand, significant star formation will only take place, as Shu *et al.* pointed out, if the unperturbed gas velocity perpendicular to the wave front,  $W_{\perp 0}$ , is greater than the speed of sound in the intercloud phase of the gas, about  $10 \text{ km s}^{-1}$ . Taking our maximum corotation radius of  $12'$  (11.4 kpc) in the southeast, we find that  $W_{\perp 0}$  drops from  $15.6 \text{ km s}^{-1}$  at  $9'5$  (9 kpc) to  $8.3 \text{ km s}^{-1}$  at  $10'5$  (10 kpc) from the center. With this in mind it is interesting to note that the most remote spiral arm H II regions measured by Münch are at  $10'2$  (9.7 kpc) in the southeast and  $9'7$  (9.2 kpc) in the northwest when account is taken of the geometry of M81. Although Münch measured one H II region  $15'5$  (14.7 kpc) from the center of M81, this object is not located on any possible extension of the spiral arms. It is very likely that it did not

form as a consequence of the pattern structure or of its dynamics.

The existence and position of an inner Lindblad resonance is critically dependent upon the shape of the rotation curve in the central regions. Unfortunately, these are the regions for which we have the least information. However, as we have noted previously in this section, at least one spiral arm can be traced to within  $2'$  from the center along the minor axis (4 kpc in the plane of the galaxy). This would imply that the inner resonance is no farther from the center than 4 kpc.

Earlier in this section we discussed a possible low-surface-density extension of arm I, perhaps through a rotation of at least  $360^\circ$ . Is this material a genuine extension of the more obvious inner arm structure, or is it a morphological coincidence? If the spiral wave is maintained by reflections, the distance to the outer Lindblad resonance may be of importance in settling this question. At this radius

$$\Omega_p = \Omega + \kappa/2, \quad (4)$$

where the epicyclic frequency  $\kappa$  may be expressed in terms of the radius and rotation velocity as

$$\kappa = 2^{1/2} \frac{V}{R} \left( 1 + \frac{R}{V} \frac{dV}{dR} \right)^{1/2}. \quad (5)$$

Differentiating the Brandt rotation function leads to

$$\frac{R}{V} \frac{dV}{dR} = 1 - \frac{3(R/R_{\max})^n}{1 + 2(R/R_{\max})^n}. \quad (6)$$

Thus as  $R$  gets very large,  $\kappa$  approaches  $\Omega$  or at the limit

$$\Omega_p = \frac{3}{2}\Omega.$$

Indeed, this is true for any rotation function of Keplerian form. Using our model rotation velocities, the maximum value of  $\Omega_p$  compatible with our data implies a radius for the outer Lindblad resonance of 14 kpc in the north and 15 kpc in the south. Hence, the maximum distance to this resonance that is consistent with our observations is 15 kpc (15'8). This radial distance is quickly exceeded by the extended spiral feature as shown in figure 7. Thus, the continuity of these weak features with the more obvious inner spiral structure, while interesting, may be entirely fortuitous. These weak clumps may have nothing to do with the normal spiral structure of M81.

### c) Kinematical Effects of the Density Wave

As a consequence of the density wave, radial and tangential streaming motions are expected to be associated with the spiral pattern. Such peculiar motions will cause "wiggles" on the observed isovels (fig. 8) in a fashion that is systematic with respect to the arms. The relationship between the appropriate experimental parameters is given by Lin *et al.* (1969). We have estimated the magnitude of these peculiar velocities using our rotation data (§ V), the arm-interarm gas density contrasts, and the pattern angular

velocities derived earlier in this section. The positions for which we have done the calculations are marked on figures 3 and 8. The streaming velocities calculated are the maximum allowed by the uncertainties in our model rotation data. In the line of sight, we find for the northeast arm 3.7 and 2.1 km s<sup>-1</sup> for the radial and tangential components, respectively. In the southwest for these same velocity components, we find 6.0 and 3.1 km s<sup>-1</sup>. As these terms are in quadrature with respect to the wave potential, their maximum combined magnitude is ~4 km s<sup>-1</sup> in the northeast and ~6 km s<sup>-1</sup> in the southwest. These velocities are too small for us to observe. It can be argued, following W. W. Roberts (1969), that shock formation will magnify these velocities. However, they would probably occur on such a small scale that the present observations would smear them out.

The data, as displayed in figure 8, indeed show some "wiggles" on the isovelocity contours, particularly in the northeast where the spiral arm is well resolved relative to the main body of M81. However, no systematic pattern of velocity perturbations is seen with respect to the well-resolved spiral structure. In regions where the angular velocity of rotation is significantly greater than the angular pattern velocity (that is, closer to the center of the galaxy), the expected streaming terms are likely to be different from those we have calculated. Unfortunately in these regions the neutral gas density is too small for reliable estimates to be made of the wave amplitude. In contrast, if we examine the spiral pattern at large radii, where it is more clearly distinguished, we approach the corotation radius where the expected streaming terms are likely to be very small. Therefore, we have an observational difficulty in testing for the existence of these peculiar velocities which are an expected consequence of the density wave.

Also, we note that many of the observed "wiggles" occur on a scale similar to the beam size. Large H I density fluctuations within the beam could cause effects as large as 20 km s<sup>-1</sup> and could, indeed, account for what is observed in figure 8.

#### VIII. DYNAMICS OF THE SATELLITE MATERIAL

##### a) *The East Companion DDO 66/Ho IX*

The east companion has been catalogued as DDO 66 (van den Bergh 1959) and Ho IX (Holmberg 1969). It is a late irregular system. According to Holmberg, its absolute photographic magnitude is -13.5 mag. However, Holmberg assumed a distance of 2.9 Mpc and a galactic absorption of ~0.38 mag. Using instead a distance of 3.25 Mpc and a galactic absorption of 0.07 mag (Sandage 1973), the corrected absolute magnitude is  $M_{pg}^0 = -13.45$  mag. (This system has been rediscussed by Bertola and Maffei 1974.)

The H I contours of the galaxy are elliptical, with the major axis at a position angle of ~146°. The H I peak is found at  $\alpha_{1950} = 9^h53^m44^s$ ,  $\delta_{1950} = 69^\circ17'30''$ . Within  $\pm 5'$  of this peak along the major axis, the velocity spread is ~140 km s<sup>-1</sup>, and at the peak we find a

velocity of 40 km s<sup>-1</sup>. However, this may not be the center of this system, and the best estimate of the systemic velocity that we can make is  $40 \pm 20$  km s<sup>-1</sup>. The major uncertainty in this velocity is in the location of the center of the galaxy. The observed velocity gradient could be caused by rotational motions. The shape of the contours in figure 3 implies an inclination angle  $I$  of at least 73°. At a radius  $R$  of 5' (4.7 kpc) the maximum observed velocity is

$$V_{\max} \sin I \simeq 70 \text{ km s}^{-1},$$

where  $V_{\max}$  is the maximum rotation velocity. Fortunately, the inclination correction to the velocity is small, and we can calculate an indicative mass for the system:

$$M_T = RV_{\max}^2/G. \quad (7)$$

This indicative mass, which is a minimum value, is of the order of  $5 \times 10^9 M_\odot$ . This value is comparable to that of the Large Magellanic Cloud, but greater than that of the Small Magellanic Cloud, whereas the minimum value derived for the total H I mass ( $0.4 \times 10^9 M_\odot$ ) is similar to that of both Magellanic Clouds. The distance-independent quantity  $M_{H\text{I}}/L_{pg}$  is the best determined ratio of parameters for this system; its value is 12. Table 3 compares some of the properties of DDO 66/Ho IX with several other late-type irregular systems, three of which are of small luminosity. The most striking feature of DDO 66/Ho IX is this very high  $M_{H\text{I}}/L_{pg}$  ratio. However, according to Fisher and Tully (private communication) low-luminosity dwarf systems tend to have higher  $M_{H\text{I}}/L$  ratios than normal late-type galaxies.

Finally, we note that there is evidence of a dynamic interaction between M81 and DDO 66/Ho IX (fig. 12) and also of a bridge of H I between the two systems (fig. 3).

TABLE 3  
COMPARISON OF DDO 66/HO IX WITH  
OTHER IRREGULAR GALAXIES

Name	Distance (Mpc)	$M_{H\text{I}}$ ( $10^9 M_\odot$ )	$L_{pg}^0$ ( $10^8 L_\odot$ )	$M_{H\text{I}}/L_{pg}$ ( $\odot$ )
DDO 66/Ho IX	3.25	4.*	0.34†	12
IC 1613.....	0.66	0.51	0.74	0.7
Sex A.....	1.0	0.70	0.53	1.4
Ho I‡.....	3.25	1.0	0.82	1.2
SMC.....	0.060	4.8	7.1	0.7
LMC.....	0.052	5.4	30.	0.2
Ho II.....	3.3	9.1	9.2	1.0

NOTE.—All distances, hydrogen masses, and corrected luminosities are taken from Roberts (1969) except for Ho I.

\* Hydrogen mass may be ~ twice larger.

† The luminosity will be increased by 33 percent if Holmberg's value for galactic obscuration is used.

‡ Distance assumed from M81 group membership. Hydrogen mass provided by J. R. Fisher and R. B. Tully (private communication, 1974). Luminosity is taken from Holmberg (1958).

### b) The Arp Ring Feature

We have suggested that the ringlike, lumpy feature that merges into M81 and DDO 66/Ho IX north following the center of M81, crosses the major axis of M81  $\sim 16'$  north of the center, and merges again into M81 in a spur north preceding the galaxy, is the H I associated with the Arp ring feature. It is obvious, however, that the H I emission is very patchy compared with the diffuse optical emission. Typically, the small clumps have H I masses of  $\sim 2 \times 10^7 M_\odot$ , while the estimated H I mass for the whole feature is  $1.2 \times 10^9 M_\odot$ , half of which is concentrated in the feature peaked  $13'$  north and  $10'$  east of the center of M81. Figure 15 shows the run of the peak velocities of the spectra along the ring feature together with the expected velocities from pure rotation in the plane of M81. The peak velocities vary between 100 and  $155 \text{ km s}^{-1}$  over the whole feature and show large discrepancies with the expected circular velocities. The ring is, therefore, not participating in the general rotation of M81. The velocity of this material is typically redshifted by  $\sim 150 \text{ km s}^{-1}$  relative to the center of M81. The uncorrected H I profile width ranges from 25 to  $45 \text{ km s}^{-1}$  along the ring. In the northeast and northwest, where the feature merges into the main body of M81, the velocities in the ring are close to the velocities expected from circular rotation in M81 (fig. 10). This may indicate that the ring is connected to the plane of the galaxy at these locations. At the point where it crosses the major axis, the projected distance of the ring is 15 kpc from the center of M81.

It might be argued that this feature is part of our Galaxy. However, the large positive velocities at which we see the associated H I together with the high latitude make this possibility very unlikely. Indeed, the high-velocity survey of van Kuilenburg (1972) does not show any feature between  $+60$  and  $+270 \text{ km s}^{-1}$  over a wide range of latitudes and longitudes around this region.

### c) The Extended Spiral Material

To the west of M81 there exist several weaker features that comprise in total a gas mass of  $\sim 5 \times 10^8 M_\odot$ . We have shown in § VII that a logarithmic

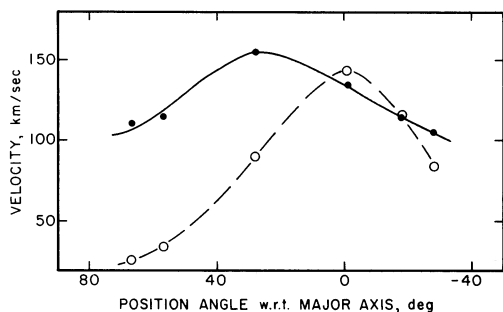


FIG. 15.—The observed line-of-sight peak velocities along the Arp ring (filled circles) compared with the expected line-of-sight velocities (open circles) from rotation in the plane of M81.

spiral with a pitch angle of  $77^\circ \pm 3^\circ$ , determined from the inner spiral structure, passes through the most intense features. However, this may be coincidental as most of these weak features are observed at radii greater than that of the outer Lindblad resonance. In any event most of this material is redshifted by 20–50  $\text{km s}^{-1}$  relative to the best circular model. These are modest noncircular terms compared with DDO 66/Ho IX or the Arp ring.

All the features discussed in this section are outlined in figure 7, showing their relation to the H I peaks, and also in figure 16, showing their relation to the observed gas column density.

Several of the most western features seen in figure 3 are too weak to show up on our model for they are at the borderline of significance. If they are real, they contain  $\sim 5 \times 10^6 M_\odot$  of neutral hydrogen and may be part of the intergalactic halo detected by Roberts (1972). Indeed, it is possible to argue that all the features discussed in this section, apart from DDO 66/Ho IX, might be part of this halo.

## IX. CONCLUSION

This study of M81 has been exceedingly fruitful, for it has revealed information about the medium surrounding the galaxy and about the spiral structure of NGC 3031 itself. One-third of the H I detected by this survey appears to lie outside the main body of M81. The largest component is the dwarf irregular galaxy, DDO 66/Ho IX, that is close to M81. The neutral-hydrogen content of this companion seems normal in relation to its indicative total mass. However, the ratio of its neutral-hydrogen mass to its luminosity is unusually high when compared with normal irregular galaxies. DDO 66/Ho IX has seriously distorted the dynamics of the south-following quadrant of M81, and the two systems appear to be connected by a bridge (see figs. 3, 6, and 12). The other components of the medium around M81 are lumpy with hydrogen masses in the range  $5 \times 10^6$ – $1 \times 10^9 M_\odot$ . These may represent large hydrogen associations, or complexes, within the tenuous intergalactic medium first observed by Roberts. In many cases the velocities of these features are vastly different from expectations if the gas is in the plane of the galaxy executing circular motion. One patchy extended feature coincides with the low-surface-brightness ring detected by Arp. The observed kinematics of this loop suggest that at each end it merges into the plane of M81. To the west of M81 are other clumps that may be associated with this ring or may be part of an extended spiral feature, a continuation of arm I.

The spiral structure of M81 is well delineated by neutral-hydrogen emission. A spiral with a pitch angle of  $77^\circ \pm 3^\circ$  fits the H I well at a radial distance of 7–10 kpc. The arm-interarm gas contrast appears to be not less than 3:1, and the arm width is  $\sim 2$  kpc. Using our data exclusively, we have derived a density-wave model for M81. This model essentially has a smaller corotation radius than the one derived by Shu *et al.* (1971) who used older optical rotation data. As a conse-

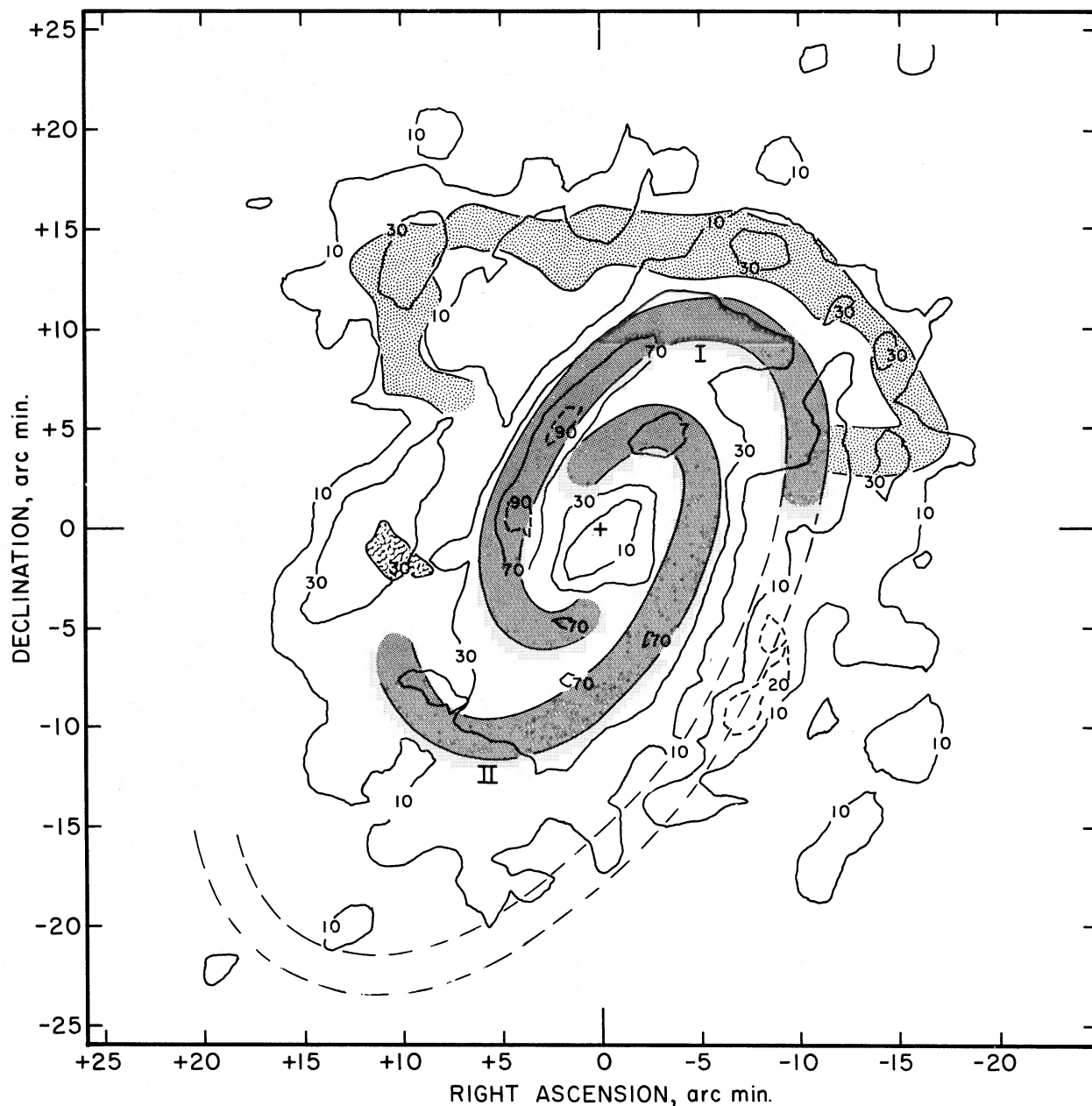


FIG. 16.—The Arp ring feature, the spiral-arm structure, and DDO 66/Ho IX are shown relative to the neutral hydrogen column density (taken from fig. 3).

quence, our model more readily explains the sharp drop in the density of H II regions at radii where there is a significant amount of H I gas still present. From the density contrast of the H I spiral arms and our density-wave model, we have calculated the magnitude of the expected noncircular velocities. These motions are too weak to be detected in the regions where the H I arms are well resolved by the present study. Indeed, our H I velocity map (fig. 8) does not show a systematic pattern of noncircular motions relative to the spiral structure.

Many of the properties pertaining only to M81 are similar to M31, but scaled down. Both galaxies are large; the radius at 10 percent of the peak H I column density is  $\sim 17$  kpc for M81 and  $\sim 26$  kpc for M31. Both galaxies are massive:  $M_T > 1.1 \times 10^{11} M_\odot$  for M81 and  $M_T > 2.2 \times 10^{11} M_\odot$  for M31 (Gottesman and Davies 1970). In their structure, both galaxies exhibit a strong central deficiency in H I, and the disks of both systems show a roughly constant  $M/L$  ratio over a large radial distance. The H I is also strongly correlated with optical spiral arms. This is

more obvious for M81, which is not as highly inclined to the line of sight as is M31 (Guibert 1974 for M31). One intriguing difference between the two galaxies is the distribution of H II regions. The maximum H I density in M81 coincides with the bright optical arms (as it does in the case of M31). However, the H I column density decreases very slowly with increasing radius in M81, whereas the surface density of H II regions drops very sharply from its maximum. This difference may be understood in terms of different density-wave models. Indeed, according to Guibert (1974), the radius of M31 with an H I density of  $2.8 \times 10^{20} \text{ cm}^{-2}$  in the plane of the galaxy is 21 kpc, barely greater than the corotation radius of 20 kpc. By contrast, our M81 model predicts a maximum corotation radius of 11.4 kpc, whereas the radius of M81 with an H I density of  $2.8 \times 10^{20} \text{ cm}^{-2}$  in the plane of the galaxy (our 20% contour in fig. 3) is  $\sim 15.8$  kpc.

We have not mentioned the 21-cm continuum emission from M81, as it has recently been discussed by van der Kruit (1973). Our data are in agreement with those observations. Table 2 lists the parameters determined by this study and discussed in this paper.

The authors are deeply grateful to Dr. M. S. Roberts for allowing them to make use of his H I data on M81, to Dr. H. C. Arp for several photographs and communications concerning the low-surface-brightness ring he had detected, and to Dr. L. A. Thompson for tabular material relating to the H II regions in M81. Dr. G. A. Tammann very kindly sent us information pertaining to the east satellite of M81, DDO 66/Ho IX. Dr. A. G. Smith kindly allowed us to make use of his photographic plates of M81.

S. T. Gottesman was a Research Associate at the NRAO when this project commenced. He is also grateful to the University of Florida Graduate School for a summer research grant and to the IAU for a travel grant to the Observatoire de Meudon in 1972, where part of this analysis was performed.

L. Weliachew was a Research Fellow with the California Institute of Technology when the observations and the data reductions were made.

Research in radio astronomy at the Owens Valley Radio Observatory is supported by National Science Foundation grant GP-30400 and by Office of Naval Research grant N00014-67-A-0094-0019.

#### REFERENCES

- Arp, H. C. 1965, *Science*, **148**, 363.  
 Bertola, F., and Maffei, P. 1974, *Astr. and Ap.*, **32**, 117.  
 Boggess, N. W. 1959, *Pub. A.S.P.*, **71**, 524.  
 Bracewell, R. N., and Roberts, J. A. 1954, *Australian J. Phys.*, **7**, 615.  
 Brandt, J. C., Kalinowski, J. K., and Rosen, R. G. 1972, *Ap. J. Suppl.*, **24**, 421.  
 Brandt, J. C., and Scheer, L. S. 1965, *A.J.*, **70**, 471.  
 Burton, W. B. 1971, *Astr. and Ap.*, **10**, 76.  
 Connolly, L. P., Mantarakis, P. Z., and Thompson, L. A. 1972, *Pub. A.S.P.*, **84**, 61.  
 Danver, C. G. 1942, *Ann. Obs. Lunds*, No. **10**, 153.  
 de Vaucouleurs, G., and de Vaucouleurs, A. 1964, *Reference Catalogue of Bright Galaxies* (Austin: University of Texas Press).  
 Gallouet, L., Heidmann, N., and Dampierre, F. 1973, *Astr. and Ap. Suppl.*, **12**, 89.  
 Gottesman, S. T., and Davies, R. D. 1970, *M.N.R.A.S.*, **149**, 263.  
 Guibert, J. 1974, *Astr. and Ap.*, **30**, 353.  
 Holmberg, E. 1958, *Medd. Lunds. Astr. Obs.*, Ser. 2, No. 136.  
 ———. 1969, *Ark. f. Astr.*, **5**, 305.  
 Hubble, E. 1943, *Ap. J.*, **97**, 112.  
 Hughes, M. P., Thompson, A. R., and Colvin, R. S. 1971, *Ap. J. Suppl.*, **23**, 323.  
 Kerr, F. J. 1969, *Ann. Rev. Astr. and Ap.*, **7**, 39.  
 Lin, C. C. 1970, in *The Spiral Structure of Our Galaxy*, ed. W. Becker and G. Contopoulos (Dordrecht: Reidel), p. 377.  
 Lin, C. C., Yuan, C., and Shu, F. H. 1969, *Ap. J.*, **155**, 721.  
 Münch, G. 1959, *Pub. A.S.P.*, **71**, 101.  
 Oort, J. H. 1965, in *Stars and Stellar Systems*, Vol. 5, ed. A. Blaauw and M. Schmidt (Chicago: University of Chicago Press), p. 473.  
 Roberts, M. S. 1969, *A.J.*, **74**, 859.  
 ———. 1972, in *External Galaxies and Quasi-Stellar Objects*, ed. D. S. Evans (Dordrecht: Reidel), p. 12.  
 Roberts, M. S., and Rots, A. H. 1973, *Astr. and Ap.*, **26**, 483.  
 Roberts, W. W. 1969, *Ap. J.*, **158**, 123.  
 Rogstad, D. H., and Shostak, G. S. 1971, *Astr. and Ap.*, **13**, 99.  
 Rots, A. H., and Shane, W. W. 1974, *Astr. and Ap.*, **31**, 245.  
 Rubin, V. C., and Ford, W. K. 1971, *Ap. J.*, **170**, 25.  
 Sandage, A. 1973, *Ap. J.*, **183**, 711.  
 Shu, F. H., Stachnik, R. V., and Yost, J. C. 1971, *Ap. J.*, **166**, 465.  
 Simkin, S. M. 1967, *A.J.*, **72**, 1032.  
 Spinrad, H., and Taylor, B. J. 1971, *Ap. J. Suppl.*, **22**, 445.  
 Tammann, G. A., and Sandage, A. 1968, *Ap. J.*, **151**, 825.  
 van den Bergh, S. 1959, *Pub. David Dunlap Obs.*, **2**, 147.  
 van der Kruit, P. C. 1974, *Astr. and Ap.*, **29**, 231.  
 van Kuilenburg, J. 1972, *Astr. and Ap.*, **16**, 276.  
 Volders, L., and Högbom, J. A. 1961, *B.A.N.*, **15**, 307.  
 Weliachew, L., and Gottesman, S. T. 1973, *Astr. and Ap.*, **24**, 59.  
 Yuan, C. 1969, *Ap. J.*, **158**, 871.

S. T. GOTTESMAN: Department of Physics and Astronomy, University of Florida, Gainesville, FL 32611

L. WELIACHEW: Departement de Radioastronomie, Observatoire de Meudon, 92190 Meudon, France